NEW DEVELOPMENTS IN ICRF ANTENNAS AND NON-TRADITIONAL APPLICATIONS OF HF POWER ON TEXTOR

A.Lyssoivan[1], A.Messiaen[1], R.Koch[1], F.Durodié[1], G.S.Amarante-Segundo[1], P.Dumortier[1], D.Van Eester[1], M.Vervier[1], R.Weynants[1], H.G.Esser[2], E.Gauthier[3], F.Hoekzema[2], V.Philipps[2], E.Westerhof[4]

[1] *Laboratoire de Physique des Plasmas / Laboratorium voor Plasmafysica, ERM/KMS, Association EURATOM-BELGIAN STATE, 1000 Brussels, Belgium*[*]

[2] *Institut für Plasmaphysik, Forschungszentrum Jülich, Association EURATOM-KFA, 52425 Jülich, Germany*[*]

[3] *Association EURATOM-CEA sur la Fusion Contrôlée, CEA Cadarache, 13108 St Paul lez Durance, France*

[4] *FOM-Instituut voor Plasmafysica 'Rijnhuizen', Associatie EURATOM-FOM, 3430 BE Nieuwegen, The Netherlands*[*]

[*] *- Partners in the Trilateral Euregio Cluster (TEC)*

Abstract

This paper reviews the present status of new developments in ICRF antennas, recent results on more realistic modeling of ICRF antennas using the 3-D full electromagnetic code ICANT and, finally, the latest development in the scenarios of non-traditional applications of HF power for wall conditioning.

1. Antenna developments

The ICRH system installed on TEXTOR consists of two double strap shielded or unshielded antennas, each fed by a 2MW generator (in the frequency band 25÷38MHz) via a transmission line [1,2]. Each antenna pair may be operated in 0 or π phasing.

New developments on ICRH antennas are being performed (**i**) to increase their RF voltage stand-off and (**ii**) to solve the problem of generator tripping with fast variation of antenna plasma loading. These innovations were undertaken with a view to testing solutions to increase the power capability and to decrease the sensitivity to ELM's of the ICRF system needed for ITER. In addition to the antenna design activity, development of the new RF diagnostic based on RF probe arrays has been undertaken with the aim of detecting (**i**) RF voltage/current at the antenna and (**ii**) RF field in the scrape-of-layer along the torus.

1.1. Low Electric Field ICRF Antenna

To achieve the first goal (an increase of the antenna RF voltage stand-off), the thin radiating straps (having a thickness of 10 mm at the edges) of one of the two pairs of TEXTOR antennas was replaced by a set of three parallel cylindrical tubes of 30 mm diameter [3] (Fig.1).

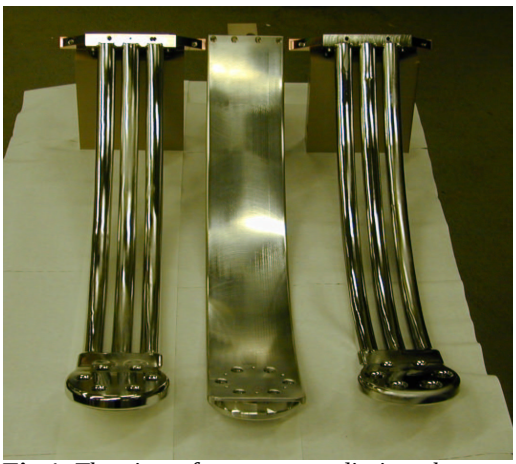

Fig.1. *The view of two types radiating elements designed for the TEXTOR ICRF antennas: standard thin strap (in the middle) and a new design of three parallel tubes.*

The driving idea for the test was to investigate if the limits in voltage stand-off of an ICRF antenna were determined by the *voltage* or by the *electric field on the edges of the inner conductors*. A 2-D electrostatic modeling [3] was used to analyze the original *thin* (T) antenna and the new *low electric field* (LE) antenna. The effect of the plasma was approximated by a conducting plane in front of the radiating elements. The modeling showed (Fig.2) that for the same voltage V_A applied to both antennas the maximum electric field (**i**) appeared at the edges of the radiating elements and (**ii**) was reduced by a factor of ~1.6 for the LE antenna.

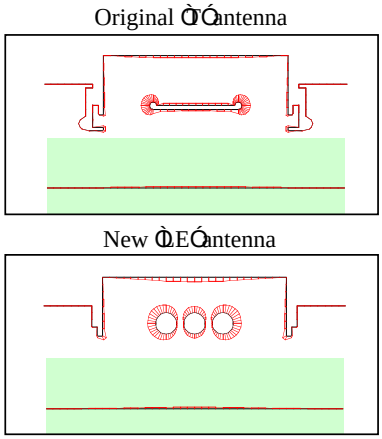

Fig.2. *Modeling of the electric field radiated by one half of the original "T" and new "LE" antennas. In each case, the amplitude of the RF field is normalized to its maximum value.*

As the RF current density is larger at the inner side of the radiating strap [4] there is a loss of coupling to the plasma (which can be expressed by the distributed loading resistance R_A) and a decrease of its distributed inductance L_A. For the given radiated power $P_{RF-A} = (1/2)G_A|V_A|^2$, the antenna conductance may be written as [1]:

$$G_A = \left(R_A l/(\omega L_A l)^2\right) f_1(\beta l), \ (R_A << \omega L_A) \qquad (1)$$

Here $f_1(\beta l) = (\beta l)^2 (1 + \sin(2\beta l)/2\beta l)/2\sin^2(\beta l)$; l is the length of radiating strap in the poloidal direction; $\beta = 2\pi/\lambda = \omega\sqrt{L_A C_A}$; C_A is the distributed capacitance. When $0 < l/\lambda < 1/4$, function f_1 has a small variation in the relevant range ($1.0 < f_1 < 1.23$) and can be considered roughly as a constant. As a result, one can obtain from (1) that, for the LE antenna, some of the decrease in R_A is compensated partially by a decrease of L_A ($G_{A\text{-LE}} \approx 70 R_{A\text{-LE}}$ μOhm^{-1} for the LE antenna and $G_{A\text{-T}} \approx 53 R_{A\text{-T}}$ μOhm^{-1} for the thin one). Figure 3 compares the

evolution of R_A with the plasma edge density for the two antennas in the same set of discharges. The ratio $R_{A\text{-}LE}$ / $R_{A\text{-}T} \approx 0.68$ and, for the same radiated power, we have $V_{A\text{-}LE}$ / $V_{A\text{-}T} \approx 1.06$.

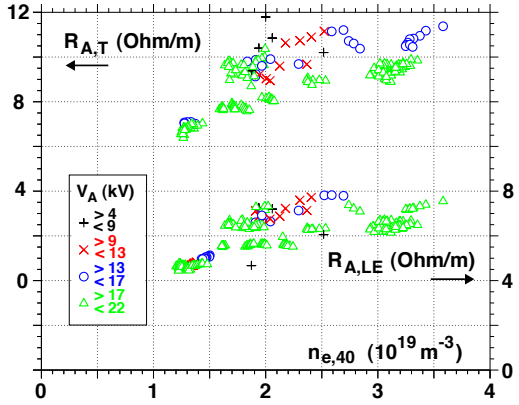

Fig.3. *The distributed loading resistance R_A vs. line averaged density near the plasma edge (at 6 cm from LCMF) analyzed for the TEXTOR shots ##91409-91445.*

The LE and T antennas have been routinely operated with high reliability up to the full installed power (2MW applied to each antenna, 95% of which were radiated). No limit in the RF voltage stand-off for both antennas has been noted so far. However, if the power limitation is assumed to be due to arcing between the strap and the antenna box one could expect an improvement in the RF power handling capability of the LE antenna by a factor $P_{A-LE}/P_{A-T} = (\tilde{E}_{A-T}/\tilde{E}_{A-LE})^2 (V_{A-T}/V_{A-LE})^2 \approx 2.3$.

1.2. Load insensitive ICRF Antenna

The other new ICRF antenna system has been designed (**i**) to be compatible with the inlet of the diagnostic neutral beam between its two radiating straps (due to the rearrangement of the diagnostic positions resulting from the Dynamic Ergodic Divertor installation on TEXTOR) and (**ii**) to be able to test a "conjugated T" mode of operation [5] that is foreseen for the new JET-ITER-like antenna [6]. The major problem of the ICRF heating of plasma in the Elmy H-mode (the basic regime for ITER) is the severe power limitation due to generator tripping which occurs in presence of ELM's. This tripping happens due to fast increase of the antenna load by the ELM's or to arcs induced by them [7]. The "conjugated T" mode is characterized by its insensitivity to the variations of the antenna loading resistance and would help to solve the problem of generator tripping.

The side and top view of the new antenna pair is shown on Fig.4. The two identical radiating straps (part A-C on Fig. 4a) are fed by their feeding lines at a tap B. They are short-circuited at one side and connected at the other side to a vacuum variable capacitor (grounded in E) by means of a section C-D of coaxial line. The two feeding lines are connected to the line coming from the generator by means of a *T junction* as shown schematically on Fig.5a). The lengths B_R-T and B_L-T between each tap and the point "T" can be adjusted by means of the line stretchers $(LS)_R$ and $(LS)_L$.

<u>*Transmission line theory analysis.*</u> The antenna set-up (Fig.5a) is easily modelled using transmission line theory: (**i**) the radiating strap by sections of lossy strip line characterized by distributed resistance (due mainly to plasma loading) R_A, inductance L_A and capacitance C_A, (**ii**) the vacuum or air pressurized parts *C-D* and *B-T* by sections of coaxial lines of appropriate characteristic impedance, (**iii**) the capacitor C_P by its capacitance and stray inductance. The behaviour of this tuneable system can be understood in terms of equations of a simplified equivalent circuit (Fig.5b).

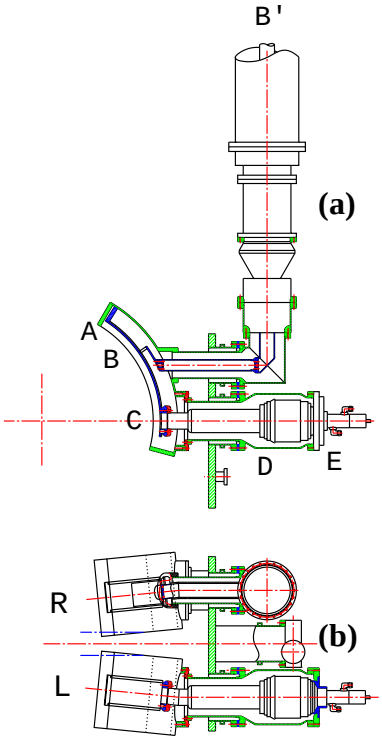

Fig.4. *The side (a) and the top (b) views of the new antenna pair. The top view shows the upper part of the antenna on the R side and the lower part on the L side, respectively.*

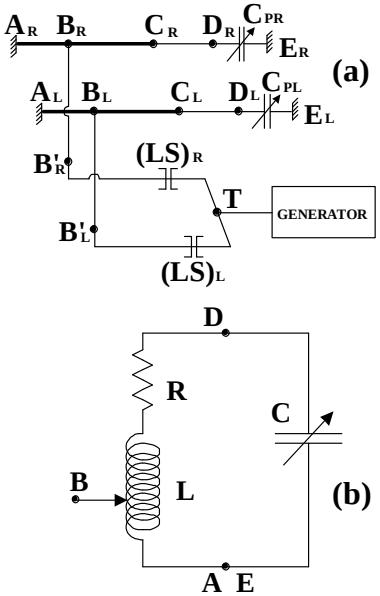

Fig.5. *The schematic diagram of the load insensitive antenna system (a) and the equivalent circuit of the tunable strap (b).*

For the frequency range used ($f \geq 30$ MHz), the line path *A-D* has an electrical length shorter than a quarter wavelength $\lambda/4$ and behaves as an inductance *L*. The part *A-E* of the antenna system is equivalent to a parallel resonating circuit fed in *B* at the fraction α of this inductance. We have $R \propto R_A$ ($R=R_A l_{A\text{-}C}$ in the limit of

short electrical length $l_{A\text{-}D}$), L depends on L_A (L_A is a weak function of the plasma loading [1]) and C is determined by C_P and its stray inductance. The impedance seen in the point B is given by:

$$Z_B = \alpha^2 (L/(CR))(1 - i2Q\Delta f / f)^{-1}, \quad (Q >> 1) \qquad (2)$$

Here f is the operating frequency; $\Delta f = f - f_{C_P}$; $f_{C_P} = (LC_P)^{-1/2}$ and $Q = 2\pi f L/R$. At the position B' along the feeder, which is at the distance $\lambda/4$ from the tap B, the normalized impedance may be written as:

$$z_{B'} = r + ix = Z_{B'}/Z_0 = Z_0/Z_B . \qquad (3)$$

Here $r = Z_0 RC/\alpha^2 L$; $x = r2Q\Delta f / f$ and Z_0 is the feeder characteristic impedance. These relations are valid for the right R and the left L straps. We have also $z_{TR}=z_{B'R}$ and $z_{TL}=z_{B'L}$, when the electrical lengths $l_{B'R-T} = n\lambda/2$ and $l_{B'L-T} = m\lambda/2$ are equal to integer numbers of the half wavelengths.

Antenna matching conditions. The normalized admittance in the point T (Fig.5a) seen from the generator is given by:

$$y_T \equiv g + ib = y_{TR} + y_{TL}, \qquad (4)$$

where $g = g_R + g_L$ and $b = b_R + b_L$. The same power is radiated by two straps when $g_R=g_L$ (**i**). The generator sees a matched load when y_T =1, i.e. when b_R= -b_L (**ii**) and $g = g_R + g_L = 1$ (**iii**). If we choose C_{PR} and C_{PL} such that $z_{B'R} \cong z^*_{B'L}$,i.e. x_R =-$x_L \equiv x$, we satisfy the conditions (**i**) and (**ii**) and we have $y_T \cong g = 2\zeta(1/x)(1+\zeta^2)^{-1}$ with $\zeta = r/x$. If additionally $|x| \cong 1$ the matching is obtained for $|\zeta|$=1 (condition (**iii**) is satisfied). These matching conditions are fulfilled when:

$$\zeta = r/x = (2Q\Delta f / f)^{-1} = \pm 1, \qquad (5)$$

$$r = Z_0 RC/\alpha^2 L = 1. \qquad (6)$$

The conditions (5) and (6) can be achieved approximately by the proper choice of C_{PR} and C_{PL} and of the tap position (i.e. by the value of α) for the reference value $R = R_0 \propto R_{A0}$, where $R_0 = 4\pi L|\Delta f|$. In this case conditions close to matching will remain in a large R or R_A range around R_0 or R_{A0} due to the small variation of the function $2\zeta/(1+\zeta^2)$ around ζ=1. The *voltage standing wave ratio* (VSWR) remains low, S<1.5, in a large range of antenna loading $0.38<R_A/R_0<2.6$. This large independence of the matching on R_A has a drawback. The phase difference $\Delta\phi$ between the current in two adjacent straps strongly depends on R_A through the relation $\Delta\phi \cong 2\mathrm{arctg}(1/\zeta) + (m-n)\pi$. Modeling of the complete set-up is shown in Figure 6.

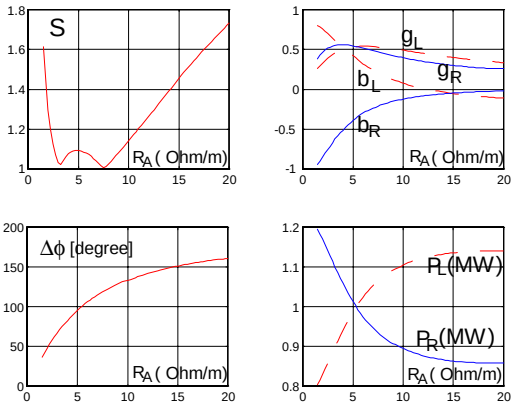

Fig.6. *The result of optimization of the "conjugated T" mode of operation for the case of TEXTOR (C_{PR}=80.4 pF, C_{PL}=67.2 pF, $l_{BR\text{-}T}/\lambda = 1.248$, $l_{BL\text{-}T}/\lambda = 1.717$, f=32.5 MHz).*

The VSWR at the generator, S, remains below 1.1 in the loading resistance range R_A≈2.5÷9.5 Ohm/m and S<1.5 in the range R_A≈1.6÷16.0 Ohm/m. It should also be noted the following outcomes of the antenna matching optimization for operation in the "conjugated T" mode:

- the normalized admittance remains close to conjugated one ($y_{TR} \cong y^*_{TL}$) in the low S range;
- the normalized conductance remains very close to 0.5 ($g_R \cong g_L \cong 0.5$);
- the radiated power becomes balanced in the straps when $g_R=g_L$;
- the phase shift between the straps changes in the small range $\Delta\phi$≈110°÷140° for a roughly doubled variation of the antenna-plasma resistance, observed in the experiment, $R_{A\text{-}T}$ ≈6.0÷12.0 Ohm/m, (Fig.3), if difference in the electrical length of the straps is equal to half a wavelength, m-n =1.

2. ICRF Antenna modeling

More realistic antenna modeling using the 3-D full electromagnetic RF code ICANT [4,8] has been undertaken (**i**) to analyze the ICRF antenna near-field in vacuum and (**ii**) to assess the antenna coupling capability as a function of the current strap thickness and position in an antenna box. This code computes the current distribution on a 3-D model of ICRF antenna self-consistently by superposing currents on each rectangular element of the antenna model and imposing the vanishing of the tangential electric field on the antenna surface. Improvements in the ICANT code have been done to allow more complicated modeling of ICRF antennas surrounded by antenna box, with finite thickness of the current straps and Faraday shield (FS). The electromagnetic problem solved in the vacuum region is matched with a surface impedance matrix calculated by a full-wave code as a boundary condition on the plasma-vacuum interface.

2.1. Analysis of the antenna near RF field in vacuum

A study of the antenna near field in vacuum is an important issue particularly in relation to optimization of the performance of ICRF wall conditioning discharges in fusion devices using conventional ICRH antennas with or without FS [9]. It is well known, that (**i**) electromagnetic waves in the ICRF band are not propagating in vacuum and that (**ii**) mainly the antenna parallel electric RF field $\tilde{E}_z$ (along the static magnetic field lines) is responsible for the neutral gas breakdown and initial ionization by e-impact [10]. In general, ICRH antennas with the radiating straps oriented in poloidal direction can generate an E_z-field in vacuum due to (**i**) RF voltage difference between the strap and the sidewalls and (**ii**) RF voltage induced between the tilted FS bars by the time-varying magnetic flux [9]. ICANT modeling of the antenna field in vacuum for the cases of TEXTOR-like unshielded antenna and that one without protecting box is shown in figures 7, 8. It is clearly seen that the $\tilde{E}_z$-field (**i**) is generated efficiently in both analyzed cases and (**ii**) is localized at the edges of the radiating straps. For the given RF current in the feeding points, I_{RF} =1 kA, the radial decay length of the field was found to be larger in the hypothetical "no box" case (Fig.8). Obviously it resulted from the absence of image currents on the surfaces of former nearby located antenna box. The conducting back-wall was present at the same distance from the straps for both cases.

2.2. Antenna coupling analysis

The possibility to model thick antenna straps has been recently implemented in the ICANT code. This

modification allows assessing more realistically the flow pattern of the current on the main conductors of the antenna. The main effect, which was investigated for the first time in modeling of the JET-ITER-like ICRF antenna [4], is the following. When increasing the thickness of antenna strap, a larger fraction of the RF current "prefers" to flow on the backside of the strap, thereby reducing the current on the front side and therefore decreasing the antenna-plasma coupling.

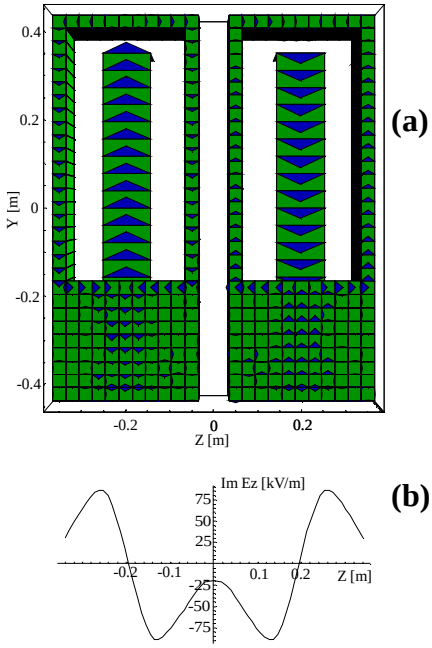

Fig.7. *Modeling of the TEXTOR unshielded antenna (f=32.5 MHz, π-phasing): (a) – the RF current distribution in the straps and boxes; (b) – toroidal distribution of the $\tilde{E}_z$-field at the coordinates: x=0.06 m; y=-0.15 m.*

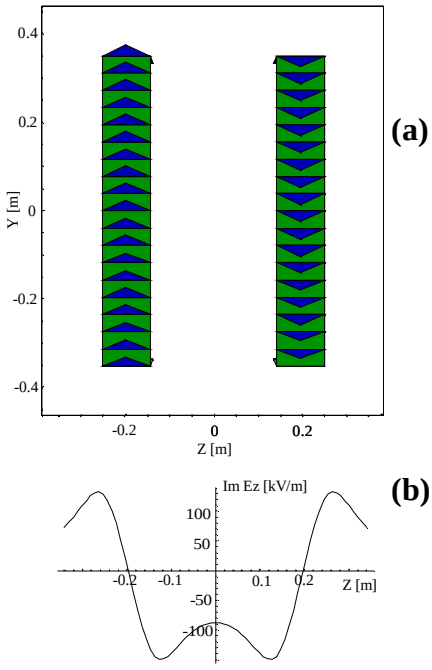

Fig.8. *The simplified model of radiating straps of the TEXTOR antenna without box (input parameters are mentioned in Fig.7).*

Modeling of the two types TEXTOR antenna radiating elements (Fig.1) resulted in the following. The three-tube radiating element (Fig.9a) caused the RF current to re-distribute towards the backsides and, partially, to the lateral sides (Fig.9b) due to larger thickness, thus reducing antenna coupling by ~12%. On the other hand, the discreteness of the tubes resulted in a more homogeneous (by ~35%) RF current distribution in the *z*-direction, compared with that of the standard strap, where nearly all the current flows at the strap edges.

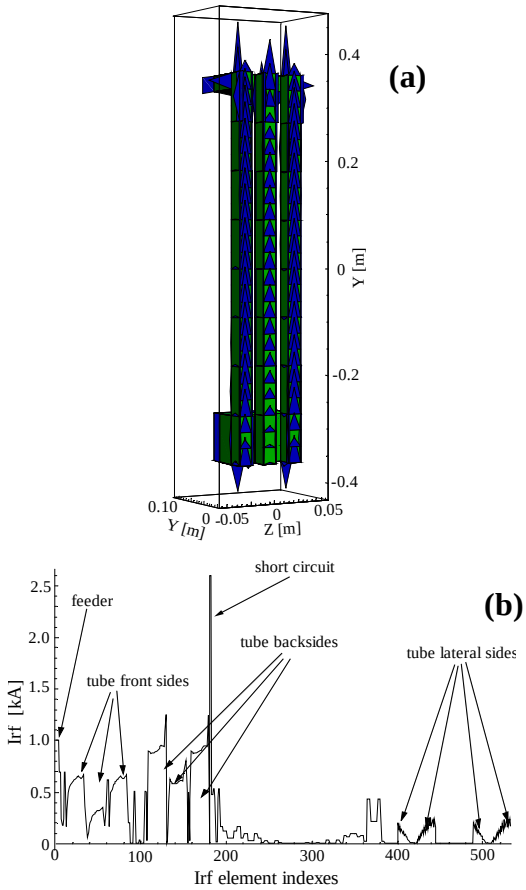

Fig.9. *The model of single three-tube radiating module of the TEXTOR LE antenna (a) and the RF current distribution for each element of the model (b) loaded by TEXTOR-like plasma: n_{e0}= 4.0×10^{19} m^{-3}, n_{ea}= 1.0×10^{19} m^{-3}, λ_{ne}= 1.0 cm.*

2.3. JET-ITER-like antenna modeling

Being in charge to build JET-ITER-like ICRF antenna with the aim to demonstrate the feasibility of high power density coupling, the Laboratory for Plasma Physics ERM/KMS made also crucial contribution into a more realistic modeling of this antenna using the ICANT code. A self-consistent solution of the electromagnetic problem in vacuum together with an input surface impedance matrix for the realistic 3-D antenna geometry revealed several major effects, like reduction of the coupling due to radiating strap thickness and poloidal phase difference between the straps, strong sensitivity of the coupling to antenna-plasma distance and central plasma density variations [4,6,8].

3. ICRF wall conditioning technique development

In future reactor-scale *superconducting* fusion devices such as ITER, the presence of permanent high magnetic field will prevent the use of *Glow Discharge Conditioning* procedures in between shots, which presently is the preferred method to decrease the content of light impurities such as oxygen and to control the

recycling properties of the Plasma Facing Components (PFC) [11]. The needs of controlled and reproducible plasma start-up and Tritium removal e.g. from the co-deposited carbon layers, will require applying an *alternative* conditioning procedure. ECR Discharge Conditioning (ECR-DC) and ICRF-DC are fully compatible with the presence of magnetic fields. ICRF-DC has already been developed in TEXTOR [12] and in TORE SUPRA [13] using the present generation of ICRF antennas, with or without FS. To develop *alternative* ITER-relevant scenarios for efficient wall conditioning in the presence of a high magnetic field, comparative studies of ICRF-DC / ECR-DC have been undertaken on TEXTOR using the present ICRH and ECRH systems *without changes in hardware* [14,15].

3.1. ECR/ICRF conditioning discharges performance

The results of the experiments clearly show the major differences in the performance of *alternative RF discharges* for the same machine parameters {B_T = (1.65÷2.28) T, $p_{He}\approx(3\div6)\times10^{-2}$ Pa, $P_{ICRF}\approx P_{ECRH}\approx$100 kW÷200 kW}.

ECRH Plasma. High density plasma ($\bar{n}_{e0}\approx2.4\times10^{18}$ m^{-3}) is initiated near the resonant layer $\omega=2\omega_{ce}$ (centred at $B_T\approx1.96$ T) and moves outside due to the $(\boldsymbol{E}\times\boldsymbol{B})$-drift in a pure toroidal B_T. Neutral gas (Helium) breakdown and ionization occur simultaneously all over the torus because of microwaves propagating in vacuum. Plasma production is only possible when the $2\omega_{ce}$ layer is present inside the vessel and with the X-mode polarization of the microwave beam. ECR discharges are strongly localized along the path of the microwave beam, which is focussed in the equatorial plane (Fig10a).

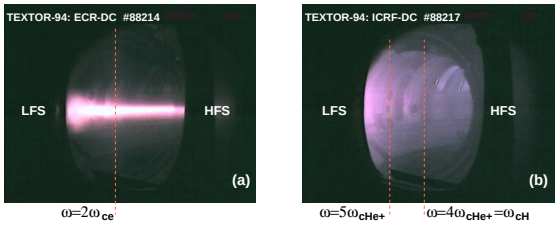

Fig.10. *The view of ECR plasma (a) and ICRF plasma (b) from CCD camera: (B_T =2.0 T, p_{He}= 3×10^{-2} Pa, P_{ICRF}=90 kW, P_{ECR}=150 kW).*

ICRF Plasma. ICRF discharge starts from neutral gas breakdown and initial ionization in the LFS antenna area (RF waves are not propagating in vacuum). It may happen when amplitude of the antenna $\tilde{E}_z$-field in vacuum satisfies the RF breakdown criterion [9,10]

$$(\omega/e)(2m_e\varepsilon_i)^{1/2}\le\tilde{E}_z(r)\le(m_e\omega^2L_z)/(2e). \qquad (7)$$

Here ε_i is the ionization energy threshold for molecules; $L_z=2\tilde{E}_z/(d\tilde{E}_z(z)/dz)$ is the parallel length scale of the ponderomotive potential. The RF breakdown time is in the range $t_{bd}\le$ 10 ms at $P_{ICRF}\approx$ 10 kW, $p_{He}\approx 3\times10^{-2}$ Pa. Shortly after breakdown (on achieving a threshold density determined by the condition $\omega_{pe}\ge\omega$), the RF plasma build-up takes place all over the torus during the remainder of the RF discharge (volume ionization during the *propagating plasma waves* phase) and is characterized by a homogeneous density profile. This is clearly seen both with a CCD camera (Fig.10b) and with the 9 channels HCN interferometer. Low-density ICRF plasmas ($\bar{n}_{e0}\approx0.4\times10^{18}$ m^{-3}) could easily be produced in the full range of tested magnetic field B_T=1.09 T÷2.30 T, gas pressure $p_{He}\approx$ (1÷7)×10^{-2} Pa and RF power $P_{ICRF}\approx$ 30 kW÷120 kW, thus confirming a predicted broad range of plasma production by the ICRF power [9].

3.2. ECR/ICRF wall conditioning efficiency

To compare quantitatively the conditioning efficiency of both techniques, the total amount of desorbed molecules integrated over 1 minute has been measured for each pulse, taking into account the calibration factor and the pumping speed for each gas. Figure 11 shows the evolution of outgassing of H_2, HD, H_2O, CO and CO_2 during a series of 5 ECR-DC and ICRF-DC, performed in similar conditions. Analysis of such studies revealed a striking result: the hydrogen removal was about 20 times higher with ICRF-DC than with ECR-DC and the light impurities such as H_2O, CO and CO_2 were not removed using the ECR discharge produced by a focused microwave beam [15].

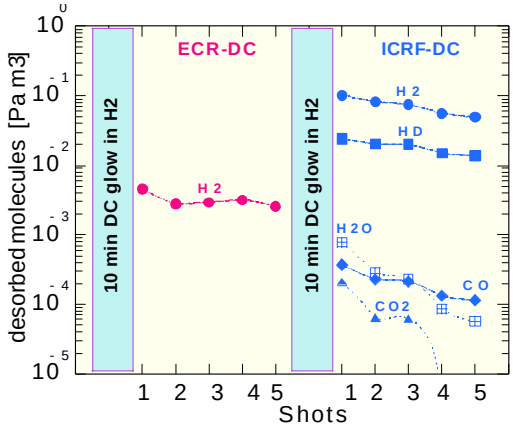

Fig.11. *Desorption rate of H_2, HD, H_2O, CO and CO_2 after a series of ECR-DC and ICRF-DC (B_T =2.0 T, p_{He} =2.5×10^{-2} Pa, P_{ECR}=150 kW, P_{ICRF}=60 kW).*

However, the combination of ECRH and ICRF power seems promising for decreasing the RF voltage at the ICRF antenna and improving the RF power coupling (up to 36%). Analytical and numerical analysis showed that ICRF-DC could reasonably be extrapolated to reactor size fusion devices. As a next step, test of the ICRF discharge performance in JET with A2 antenna is planned.

References

1. Messiaen A., et al., *Plasma Phys. and Contr. Fusion*, **31** (1989) 921-939.
2. Van Nieuwenhove R., et al., *Nuclear Fusion* **32** (1992) 1913-1925.
3. Messiaen A., et al., in *Proc. 29th EPS Conf. on Plasma Phys. and Contr. Fusion,, Montreux 2002, ECA Vol.***26B,** *paper* P-2.062.
4. Amarante-Segundo G.S. and Koch R., in *Proc. 29th EPS Conf. on Plasma Phys. and Contr. Fusion,, Montreux 2002, ECA Vol.* **26B,** *paper* P-2.041.
5. Goulding R.H., et al., *Bull. Am. Phys. Soc.*, **46** (2001) No.8, p.154.
6. Durodié F., et al, in *Proc. AIP 14th Topical Conf. on Radio Frequency Power in Plasmas, Oxnard 2001, Vol.* **595**, p.122-125.
7. Wouters P., et al., *IEA workshop on ELM's , Culham, June 2002.*
8. Pecoul S., et al., *Computer Physics Communications* **146** (2002) 166-187.
9. Lyssoivan A., et al., *Final Report on ITER Subtask* D350.2 *Part* I (1998) "*ICRF Wall Conditioning*".
10. Lyssoivan A., et al., *Nuclear Fusion* **32** (1992) 1361-1372.
11. Winter J., *Plasma Phys. Control. Fusion* **38** (1996) 1503-1542.
12. Esser H.G., et al., *Journal of Nuclear Materials* **241-243** (1997) 861-866.
13. De la Cal E. and Gauthier E., *Plasma Phys. and Contr. Fusion* **39** (1997) 1083-1099.
14. Lyssoivan A., et al., in *Proc. AIP 14th Topical Conf. on Radio Frequency Power in Plasmas, Oxnard 2001, Vol.* **595**, p.146-149.
15. Gauthier E., et al., in *Proc. 28th EPS Conf. on Contr. Fusion and Plasma Phys., Madeira 2001, ECA Vol.* **25A,** *paper* P-5.094.